Double-Walled Carbon Nanotubes Ink for High-Conductivity Flexible Electrodes

Atif Aziz,* Mohamed Basel Bazbouz, and Mark Edward Welland

ACCESS | 📊 Metrics & More | 📰 Article Recommendations | 🆂�🅸 Supporting Information

MICROFLUIDIZER

IN → OUT

Recycling tube, Reservoir, Hydraulic cylinder, Sample Chamber, Micro channel, Cooling bath

500nm
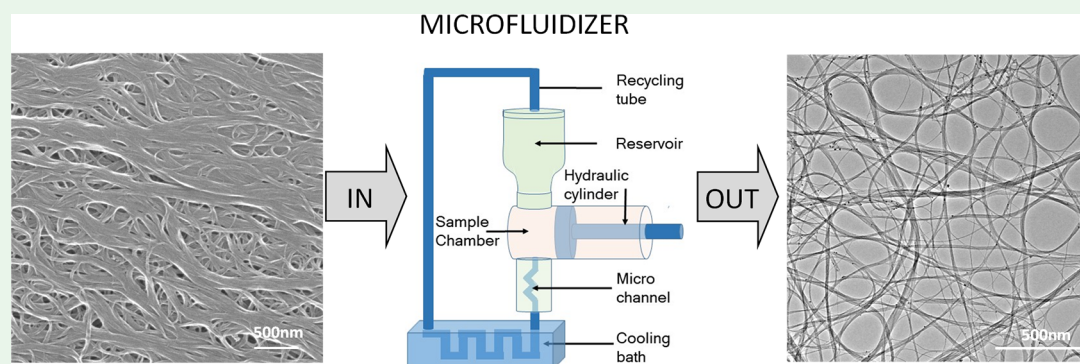
ABSTRACT: Carbon electronics is a growing field that spans printable electronics, energy storage devices, and biosensors. The commercialization of these carbon-based technologies requires a scalable production of high-conductivity, acid-free carbon nanotube ink dispersions. Superacids have been used to achieve high-concentration CNT inks; however, a scalable acid-free process to achieve similar concentrations has been missing for a long time. In this work, we demonstrate that water and sodium cellulose are sufficient for achieving a scalable production of highly conductive CNT-based ink, provided the solution is processed through a very high-shear microfluidizer. Materials used in this process are acid-free and require no postprocessing, such as centrifuging or heating. We have achieved conductivity and sheet resistance of $(3.6 \pm 0.2) \times 10^5$ S m^{-1} and 0.11 $\Omega \square^{-1}$ mil^{-1}, respectively, which are among the best reported values for any undoped carbon-based film. The thermal conductivity of the free-standing carbon films is 43 ± 4 W m^{-1} K^{-1}. By use of this method, uniformly dispersed CNT inks of viscosity >1 Pa·s are produced. Once printed on paper, these CNT films show pronounced resilience to mechanical deformation. This simple but scalable process provides a viable technology for using carbon-based conducting inks for printing large-scale devices.

KEYWORDS: double-walled carbon nanotubes, dispersion, conductivity, microfluidization, sheet resistance

INTRODUCTION

CNT-based technologies have seen tremendous progress over the past two decades. Because of excellent electrical, mechanical, and chemical properties, CNTs have found research applications in gas/chemical sensors,[1] biosensors,[2] hydrogen storage,[3] printable electronic devices,[4] composites,[5] flexible and stretchable electronic components,[6] wearable electronics,[7] supercapacitors,[8] actuators,[9] transparent electrodes,[10] and lightweight conducting wires.[11] However, commercially viable products are still scarce due to the shortage of a facile, environmentally friendly, simple, industrially compatible, and scalable process for CNT dispersion. Furthermore, the use of carbon-based materials as commercial printable conductors has been unattractive due to insufficiently low electrical conductivity. Microwave sonication, centrifugation, surfactant removal, washing, and temperature treatment are some of the most common steps used for dispersing CNTs.[12] Relying on these processing steps is generally not a problem when dealing

with a few milliliters of sample. However, when dealing with industrial-scale quantities, it is either practically not feasible or commercially not viable to use these techniques. For example, sonication is not uniform and can take a very long time, a centrifuge can only easily handle small quantities, washing steps add cost, and temperature treatment can limit the use of substrates and materials. Additionally, iodine[13] and strong acids[14] are sometimes used for dispersing and enhancing the conductivity of CNT; however, because of unstable doping and hazardous process conditions, their applications are limited. An acid- and iodine-free, environmentally friendly
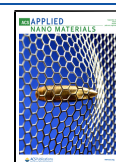
process is desirable for making printable CNT devices at scale. Along with scalability, achieving a high concentration of CNT dispersion and high electrical conductivity is also extremely important for competing with existing technologies such as silver inks. The main motivation of the paper is to provide an additional dispersion process that is water-based and provides a very high-concentration uniform dispersion of CNTs.

Figure 1 compares the best reported sheet resistances values, to date, of the films made with multiwalled CNT
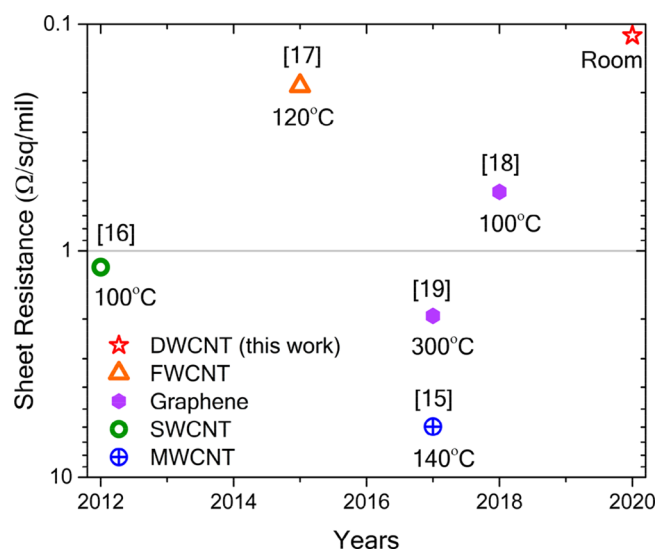
Figure 1. Comparison of the best reported sheet resistance values of MWCNT, SWCNT, FWCNT, and DWCNT.

(MWCNT),[15] single-walled CNT (SWCNT),[16] few-walled CNT (FWCNT),[17] and graphene (GR)[18] based conducting inks with our results of double-walled CNT (DWCNT). For comparison only, undoped films are presented except for the FWCNT film, where no undoped film results were available. These values are normalized to per mil thickness, where 1 mil = 25.4 μm. A wider spectrum of sheet resistance and conductivity results, reported in the literature, are presented in the Supporting Information.

Conducting films made with MWCNT (number of walls >4) generally has a much higher sheet resistance than SWCNT, FWCNT, and GR. The lowest sheet resistance reported for SWCNT and MWCNT films is about 1 $\Omega \ \square^{-1}$ mil^{-1} [16] and 6.7 $\Omega \ \square^{-1}$ mil^{-1},[15] respectively. For an HNO$_3$-doped FWCNT, the best sheet resistance is 0.19 $\Omega \ \square^{-1}$ mil^{-1}.[17]

Graphene ink formulations have also shown great progress over the past few years and demonstrated commercial-scale processability. The best sheet resistance of GR film achieved to date is 0.55 $\Omega \ \square^{-1}$ mil^{-1}.[18] Microfluidization has also been successfully used for creating GR inks with a sheet resistance of 2 $\Omega \ \square^{-1}$ mil^{-1}.[19] Although the sheet resistance is higher than the best value, it has an additional benefit of achieving commercial-scale production, thanks to the microfluidizer. The work presented in this paper reports the best sheet resistance value of any carbon-based films. We achieve this using an excellent dispersion of DWCNT. Figure 1 also compares the temperature treatment values of these best-reported values. In comparison, the process reported in this paper does not require any post temperature treatment. The process reported here focuses on high-concentration CNT dispersions for

making conducting electrodes, and the process maintains the integrity and intrinsic properties of the CNTs.

CNT Dispersion. Conducting films made with poorly dispersed CNTs have discontinuous conducting regions leading to broken conduction paths and therefore low and unpredictable conductivity. To overcome this problem, uniform dispersion is imperative for creating optimum conduction paths and achieving low sheet resistance and high conductivity. The concentration of CNTs in the dispersed solution also plays a very important role in tuning its rheology. For example, screen (graver) printing requires the viscosity to be from 1 to 10 Pa·s (0.1 to 1 Pa·s) and also shear thinning behavior which reduces ink spreading during the printing process.[20]

Bath and tip sonication are the most common tools used for dispersing CNTs. Ultrasound waves of frequency greater than 20 kHz are generated, and the cavitation process, i.e., the process of bubble formation, their growth, and collapse, generates local shock waves and fracture CNT bundles. Further dispersion is achieved through chemical agents, creating electrostatic repulsion, in solution.[21] However, sonication has many limitations. For example, the amplitude of the sound waves is not uniform in the solution; therefore, depending on whether CNTs are near the node or antinode of the sound field or their distance from the sonicator rod, they experience a very different dispersive force. The amplitude also dissipates very quickly when the density/concentration of the solution is high.[22] This results in nonuniform CNT dispersions.[23] This is particularly a significant problem when dealing with a large quantity (i.e., liters) and high CNT concentration solutions. To overcome these problems, a very efficient method has been developed here, which uses microfluidization, for dispersing a high concentration of CNTs in water. Water has been selected as a dispersing medium because it is environment-friendly, nonhazardous, and compatible with most industrial processes and equipment.

Microfluidization. A microfluidizer (MF) consists of two key components: a microchannel of hydraulic diameter tens of micrometers and a hydraulic system that applies a large pressure of thousands of psi to the solution to push it through the microchannel, as shown in the schematic diagram in Figure 2. The solution experiences a very high shear of the order of $10^6 - 10^8$ s^{-1} during the MF process.[19] The most important advantage of using MF is that all the CNTs present in the solution experience the same shear force during dispersion, which is not possible to achieve by using conventional sonication methods. In our experiment, the microchannel had a hydraulic diameter of 200 μm, and the process was performed at 5000 and 10000 psi. If the particles present in the solution are larger than 200 μm in diameter, the system can be blocked. After every 6 s, the hydraulic system pushes 6 mL of solution through the microchannel. We determine that at 10000 psi (6.7×10^7 Pa) it takes 1 s to force 6 mL of CNT/water solution through this channel. The system takes 5 s to reset before the next push. The total processing time is 1 mL s^{-1} cycle^{-1}, and the volumetric flow rate is 6 cm^3 s^{-1}. From the hydraulic diameter and the volumetric flow rate, the mean channel velocity (U) is inferred to be 190 m/s.

An estimated shear rate ($\dot{\gamma}$) inside the microchannel is 2.74 $\times 10^7$ s^{-1}. Detailed calculations for the shear rate and Reynolds number are given in the Supporting Information. In comparison, the rotator stator[24] and kitchen blenders[25] apply a shear rate of the order of 10^4 s^{-1}, and the shear force is
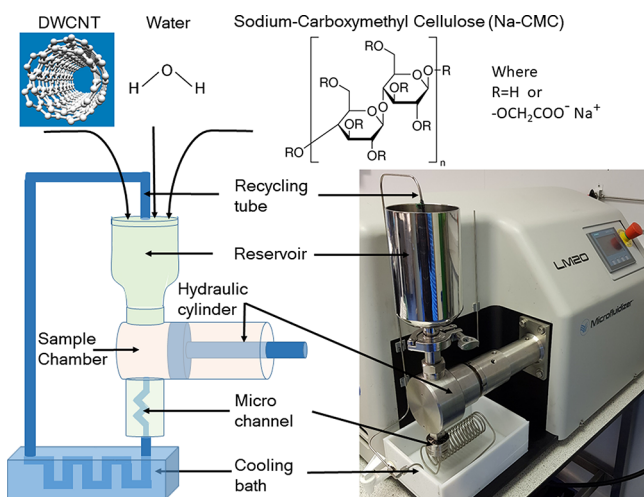
Figure 2. Right: image of the LM20 microfluidizer system used for this experiment. Left: schematic diagram of the system. Top: chemicals used in dispersion.

Figure 3. Scanning ion microscope (SIM) images of the CNT/Na-CMS/water dispersion at cycle 0 (a, d), cycle 1 (b, e), and cycle 6 (c, f). Panels a−c are the low-magnification images, whereas panels d−f are the high-magnification images. (e1, e2, e3) TEM images of the CNT dispersion after cycle 6 and pressure 10K psi.

localized between the rotation plated or near the blade. The Reynolds number ($Re = \rho u D/\mu$) is estimated to be 38000. A very high value of Reynolds number shows that the liquid flow through the microchannel is turbulent.[26] It shows that at 10K psi the solution experiences a very strong turbulent flow inside the microchannel, and the eddy currents are the main source of dispersion especially during the first few cycles. Here we define one cycle such that all the solution is passed through the microchannel once. The solution is cycled through the MF channel multiple times for best dispersion. It is observed that the viscosity of the solution increases with the number of cycles. Therefore, one may expect the Reynolds number to drop with the number of cycles.

■ RESULTS AND DISCUSSION

Figure 3 shows the scanning ion image (SIM), obtained with helium ions, of CNT dispersions at cycle 0, 1, and 6, where cycle 0 represents the initial state of the solution before it is passed through the MF. The solution is prepared by mixing 0.5 wt % DWCNTs and 0.3 wt % of sodium carboxymethyl cellulose (Na-CMC) in deionized (DI) water magnetically stirred overnight. Na-CMC is a linear polymeric derivative of cellulose. Its structure is based on the β-linked glucopyranose polymer of cellulose with varying levels of carboxymethyl ($-OCH_2COO^-Na^+$) substitution. Na-CMC used in this experiment has a substitution of 0.9. When it is dissolved in water, an electrolytic process takes place to separate a CMC molecule into sodium cations and a polymer anion which interact through electrostatic forces, which can also help in dispersing CNTs.[27] Na-CMC was used as a multifunctional additive, functioning as a dispersing agent, dispersion stabilizer, and a binder. Pluronic F-127 and poly(vinyl alcohol) (PVA) which are also water-based dispersing agents have also been tested, but the best dispersion was obtained by using Na-CMC.

Figure 3a is a SIM image of CNTs after 24 h stirring, where CNTs are all bundled together. It shows that magnetic stirring and Na-CMC alone are not sufficient for effecting dispersion. Figures 3b,e are images taken after the solution is passed through the MF chamber only once (cycle 1). It shows that even after one cycle, the CNTs start to debundle and are partially dispersed. The CNT Na-CMC solution is passed
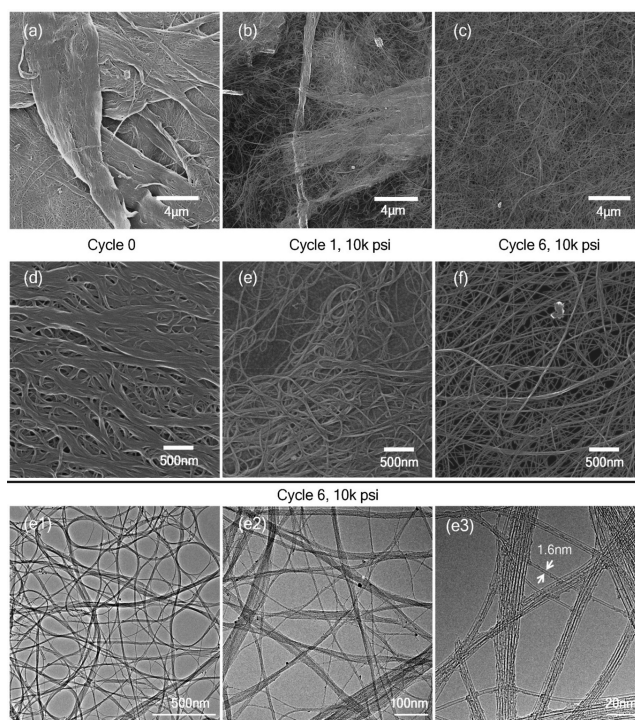
through the MF for an additional five times. Figure 3e (3f) is the low (higher) magnification SIM image of the dispersed CNTs after cycle 6. Figures 3e1−e3 are the TEM images of the same sample at different magnifications. Figures 3c,f,e clearly demonstrate that the majority of the CNTs are uniformly dispersed into smaller diameter bundles. Individual CNTs are observed in TEM images, but the majority of the bundles have diameters from 5 to 15 nm. The distribution of the diameters of dispersed CNTs is shown in Figure S2. Furthermore, the length of CNTs is of the order of micrometers with the majority having a length of about 5 μm, as shown in more detail by using TEM images presented in Figure S3. When CNTs are passed through the microchannel, they experience a very strong shear force; during this time they momentarily get separated, and the gap is filled with the Na-CMC polymer chains, which keep them separated even when the shear force is not present. Na-CMC is a polymer; its chains are attached and wrapped around the CNT surface and lead to the physical separation and electrostatic repulsion between the CNTs and cause them to disperse.[28] It is observed in the TEM images (Figure 3e3) that polymer chains only partially cover CNTs, allowing neighboring CNTs to have direct contact with each other, which is one of the possible reasons for achieving such a good conductivity despite the presence of the CMC polymer. Indeed, when the CMC polymer is removed, the conductivity of the CNT wires is increased even further.

Gravimetric measurements of the sediments, i.e., measuring the weight of the residues after centrifuging, can provide a direct measure of the dispersion efficiency of the dispersion process. To perform these measurements, samples have been collected in a 2 mL vial after cycles 0, 1, 3, 6, 9, 12, 15, and 20. These samples were then centrifuged at 10000 rpm for 10 min.
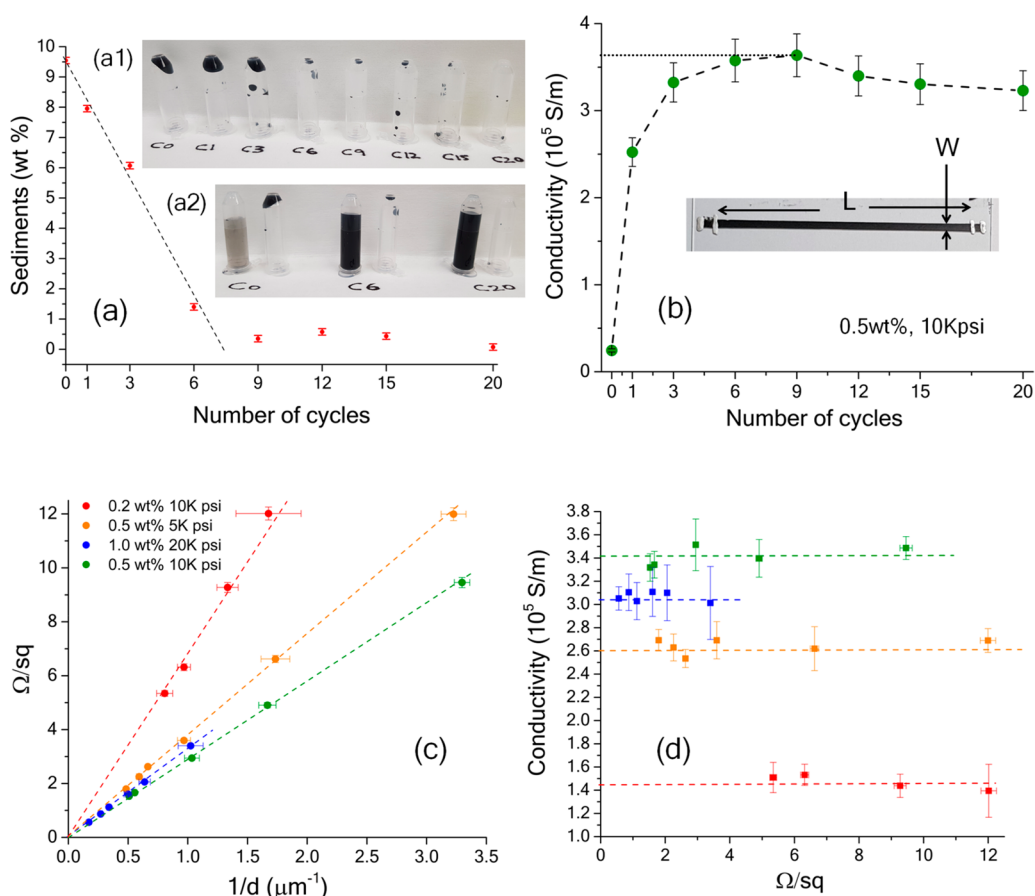
Figure 4. (a) Weight percentage of the DWCNT sediments after the centrifuge process is drawn as a function of the number of cycles the dispersing solution is passed through the MF. (a1) Residues left after cycles 0, 1, 3, 6, 9, 12, 15, and 20. (a2) Comparison of the dispersion after cycle 0, 6, and 20. (b) Conductivity of the films as a function of the number of cycles. The inset is an optical image of a typical device used to performing conductivity measurements. (c) Sheet resistance is drawn as a function of an inverse thickness of dispersions prepared at different pressures and CNT concentrations after cycle 6. (d) Conductivities of the films obtained from (c) are drawn as a function of their sheet resistances. The primary source of error is the variation in the thickness along the length of the printed wire. Error bars are due to the SD in the thickness of the films, which was measured at three different points.

During the centrifuge process, undispersed CNTs are sediment at the bottom of vial, and the dispersed CNT solution is decanted to an empty vial. Vials were weighed carefully during every stage of this process. Figure 4a is the weight percentage of the residues left in the vial as a function of the processing cycles. Figure 4a1 shows the sediment left in the vial after cycles 0, 1,3, 6, 9, 12, 15, and 20. Figure 4a2 compares the dispersed CNT solution and their sediments for cycles 0, 6, and 20. At cycle 0 a negligible amount of CNTs is dispersed in the water, whereas at cycle 20 almost all the CNTs are dispersed. Figure 4a shows that there is a sharp decline in the sediment weight as the solution is cycled through the MF. After cycle 6 more than 85% of the CNTs are dispersed, and the rate of sediment accumulation is decreased significantly. Gravimetric or centrifuge tests shown in Figure 4a were suitable only for the 0.2 wt % CNT solution; for 0.5 and 1 wt %, the viscosity of the solution was too high to perform these measurements. Therefore, to understand these dispersions, conductivity, and viscosity were measured as a function of MF processing cycles. For all the solutions Na-CMC was kept at 0.3 wt % of the total solution. Na-CMC of wt % 0.1 and 0.2 were also tested, but 0.3 wt % was the minimum quantity which gave us the stable dispersion. It remained stable for at least 3 months at room temperature. Raman spectroscopy and

FTIR measurements were also performed which can shed light on any surface damage/defects caused during the MF process.

For these experiments, we used a 150 mL solution, and the total time required to disperse 150 mL of the solution was 900 s at a rate of 1 mL cycle^{-1} s^{-1}. The scalability of our process is due to the used for microfluidization, which is inherently a linearly scalable process. In our lab we have created up to 0.5 L of dispersion, which took about 1 h. The same process can be run for as many number of times to achieve liters of dispersion solution. The solution production rate was 0.6 L/h, which was very fast as compared to existing dispersion techniques such as tip/bath sonication.[29] The processing time regime of microfluidization is very different than the sonication methods. A comparison between the process time of MF and sonication is presented in Figure 2c of ref 29, which shows that the MF process is about an order of magnitude faster than sonication. This production rate (0.6 L/h) is obtained by using only one microchannel; however, the MF process can be further scaled up by using multiple parallel microchannels. For example, the M710 multichannel microfluidizer can provide a flow rate of up to 34 L min^{-1} at 10000 psi.[30] The process presented in this paper can easily be adopted by a multichannel system, making our process truly an industrial-scale process.
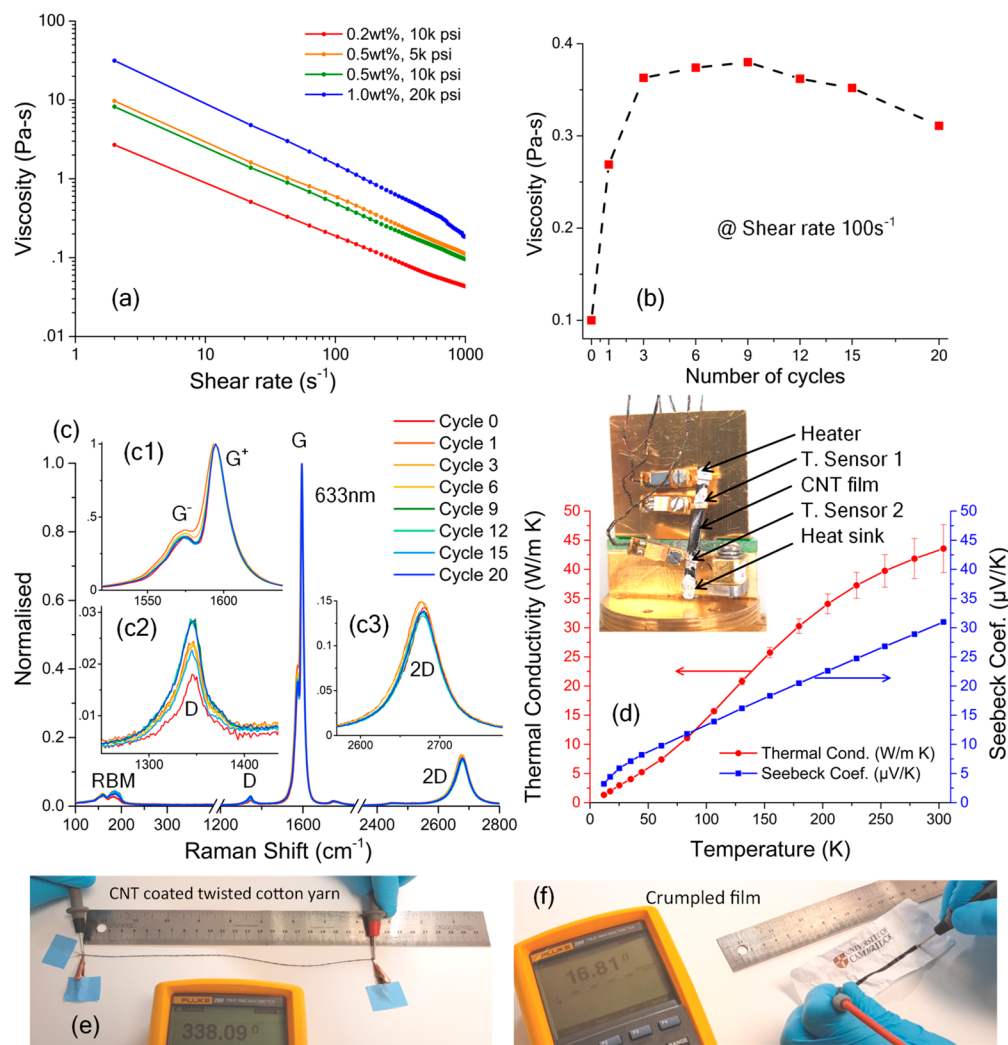
Figure 5. (a) A log−log graph of the viscosity of the CNT dispersions obtained at 5K, 10K, and 20K psi pressure and CNT concentration 0.2. 0.5, and 1.0 wt % vs shear rate. (b) Viscosity of 0.5 wt % CNT dispersion obtained at 10K psi is drawn as a function of the processing cycles at the shear rate 100 s^{-1}. (c) Raman shift spectra as a function of processing cycles. Insets show the zoomed in region near the G peak (c1), D peak (c2), and 2D peak (c3). (d) Thermal conductivity and Seebeck coefficient of the CNT film. The inset shows the micrograph of the measurement setup. Error bars are due to the error in heater current, due to a digital−analog converter, an estimated error in sample radiation (20% error), and the thermal conductance leak from the shoe assembly (10% error). (e) Resistance of the DWCNT-coated twisted cotton thread, shown in Video S1. (f) Resistance of a DWCNT-coated film on a paper after being crumpled, shown in Video S2.

Conductivity. Figure 4b shows the conductivity of the 0.5 wt % CNT films as a function of the processing cycle. At cycle 0, CNTs are not dispersed, and because of the nonuniformity of the films, conductivity is very low. As the CNT solution is passed through the MF once (cycle 1), CNTs start to disperse and the conductivity starts to increase. The conductivity reaches the maximum value for dispersions obtained after cycles 6 and 9. With every processing cycle, CNTs are more dispersed. However, at the same time, because of the large shear force, CNTs also break, increasing the number of contacts between CNTs and therefore decreasing the conductivity. These competing processes lead to maxima in conductivity as a function of the processing cycle. The maxima indicate an optimum condition for achieving the best dispersion and conductivity. The maximum conductivity achieved after 9 cycles is $(3.6 \pm 0.2) \times 10^5$ S m^{-1}, which is the highest conductivity reported for an undoped, acid-free carbon film. When these DWCNT films are soaked in HNO$_3$ for 1 h, which removes Na-CMC, the conductivity is increased

to about 7×10^5 S m^{-1}. As shown in Figure 4a, the sediments are almost 1% or less for cycles 6 and above; therefore, no centrifuge process was required to filter the dispersion for making transport devices. We used 100% of the added DWCNTs as a dispersed ink. It not only makes it straightforward to calculate the concentration of the ink but also eliminates any CNT waste generation.

Figure 4c shows the sheet resistance of the DWCNT dispersion for a CNT concentration of 0.2, 0.5, and 1.0 wt %. To compare these concentrations, devices similar to one shown in the inset of Figure 4b were fabricated by using blade coating. The length divided by the width (L/W), where $L \gg W$, is used to calculate the number of squares, which leads to the sheet resistance per unit square ($\Omega \; \square^{-1}$). Devices were fabricated with different thicknesses (d) of CNT films, and the sheet resistance was drawn as a function of the inverse thickness ($1/d$), as shown in Figure 4c. A linear dependence is observed for all the devices, and the slopes give the conductivity of the CNT films. The 1.0 wt % CNT solution

was dispersed by using 20000 psi because 10000 psi pressure was not strong enough to push such a high concentration of CNT solution though a 200 μm channel. The 0.5 wt % CNT solution was also processed at 5000 psi for comparison.

Figure 4d shows that the conductivity does not change significantly with the thickness of the film. This demonstrates that CNTs are evenly dispersed and form a very uniform conducting film. Among these samples, 0.5 wt % CNT dispersed in water and processed at 10000 psi had the highest conductivity.

Viscosity. Dynamic viscosity of the CNT dispersion solutions is measured by using a plate-to-plate rotational rheometer from a shear rate of 2−1000 s^{-1}. Figure 5a shows the dynamic viscosity of the dispersions used for making conducting films presented in Figure 4c. For 0.5 wt % CNT dispersions, the viscosity at a shear rate of 2 s^{-1} is about the same as honey ($\sim$10 Pa·s) at room temperature.[31] These measurements show a clear shear thinning behavior and the viscosity of the solution increases with the CNT concentration. In the case of a polymer solution, this shear thinning behavior is caused by the disentanglement or stretching of the polymer chains[32] and the alignment of CNTs in the direction of flow.[33] Figure 5a shows that the viscosity μ and the shear rate $\dot{\gamma}$ follow the Ostwald−deWaele power law $\mu = m(\dot{\gamma})^{n-1}$ for up to shear rate 500 s^{-1}.[34] At higher shear rate the viscosity deviates from the linear fit, especially from 1.0 wt % solution, which can be due to structural changes such as breaking of polymer chains or CNTs. For 0.2, 0.5, and 1.0 wt %, flow behavior index n is 0.33, 0.28, and 0.21, respectively, where a smaller n means more shear thinning. This shows that as the CNT concentration is increased, the dispersion shows relatively stronger thinning behavior. Furthermore, the viscosity of the 0.5 wt % CNT solution processed at 5000 psi is higher than the solution processed at 10000 psi. It shows that higher pressure (10000 psi) has caused more CNTs to break. It is also observed that the viscosity depends on the number of times the solution is passed through the MF. Figure 5b shows the viscosity of the solution which consists of 0.5 wt % CNT processed at 10000 psi, as a function of processing cycles, measured at a shear rate of 100 s^{-1}. The as-prepared solution (cycle 0) has the lowest viscosity. As the solution passes through the MF multiple times, the viscosity of the solution is increased. The viscosity of the solution as a function of the number cycles follows the same trend that was observed for the conductivity of the films shown in Figure 4b. A competition between the dispersion of CNTs and the breaking of CNTs due to a shear force also results in maxima in the viscosity. As CNT breaks, their hydrodynamic radius reduces, which decreases the viscosity of the solution.

Measurements of the viscosity and the conductivity as a function of processing cycles allowed us to identify an optimum processing window. It is concluded that the best dispersion and conductivity can be achieved when the DWCNT/Na-CMC/water solution is processed in the MF six to nine cycles using 10000 psi pressure. After this, dispersion is ready to be used, and no further processing steps, like filtration or centrifuge, are required. Although it is not discussed in this paper, the same method has also been successfully used for dispersing MWCNTs. Furthermore, dispersed solution can easily be diluted into lower concentrations by using physical shaking or vortex mixing.

Raman Spectroscopy and Thermal Conductivity. To investigate whether the MF process causes any surface damage

to the DWCNTs, Raman spectroscopy was performed as a function of MF processing cycles. Figure 5c shows the Raman spectrum of 0.5 wt % CNT dispersions after MF cycles 0, 1, 3, 6, 9, 12, 15, and 20. These samples are processed at 10K psi. Dispersions were blade coated on a glass substrate. After the film is dried at ambient conditions, the Raman spectra were obtained by using a 633 nm (1.95 eV) laser source. For comparison, all the spectra are normalized to the G peak. Insets show the magnified regions around the Raman shifts of D, G, and 2D peaks. Radial breathing modes show peaks below 200 cm^{-1} originating from the outer walls of DWCNTs. Signals from the inner wall are very weak. However, when Na-CMC is removed after treating with HNO$_3$, Raman shifts from the inner tubes are much more visible, as shown in Figure S3. G peaks shown in Figure 5c1 are split into G+ and G− modes of inner and outer tubes. Most importantly, the ratio of the D/G peaks has very slightly increased from 0.017 for an as-received sample to 0.025 (and 0.028) for cycles 1, 3, 6, 9, and 12 (cycles 15 and 20). Overall D/G ratios are very small, suggesting that not only the as-received DWCNTs had low defects but also the MF process did not cause surface damage to the CNTs. MF has also been used before in combination with an ultrasonication for dispersing CNTs, but significant surface damage to the CNTs during microfluidization was observed, possibly due to very low CNT concentration (0.016 mg/mL) and the use of very high pressure of 30000 psi.[29] We have observed that the high CNT concentration, high viscosity, and low processing power limit the surface damage to CNTs. In addition, no surface modification occurred during the MF process as confirmed by the FTIR measurements, which are presented as Figure S4.

The thermal conductivity and the Seebeck coefficient of a 10 μm thick film are measured as a function of temperature. At room temperature the CNT film has a thermal conductivity of 43 ± 4 W m^{-1} K^{-1}, and the Seebeck coefficient is 31 μV K^{-1}. The thermal conductivity measurement procedure is explained in more detail in the Supporting Information.

To demonstrate that DWCNTs are uniformly dispersed and can form a conformal coating on a very rough surface, 1 m 100% single cotton yarn (80 N m) that served as a core and a substrate was dip-coated with 0.5 wt % DWCNT dispersion. After drying in ambient conditions, cotton thread was folded and Z and S twisted to form a 4 ply DWCNT-coated yarn. A video of the coating and yarn formation is given in the Supporting Information (Videos S1 and S2). Figure 5e shows that the resistance of a 22.5 cm twisted yarn is 338 Ω, demonstrating that a very conductive and a conformal coating is formed on a very nonuniform surface of cotton yarn, made possible due to the uniform dispersion of CNTs.

DWCNT wires were also printed on conventional 80 g m^{-3} printing paper. A 74 mm long, 3 mm wide, and about 4 μm thick wire had a resistance of 16.1 Ω. Only a very small increase in the resistance of the printed wire is observed when the paper is folded and creased. Even after the paper is crumpled, the resistance is marginally increased to 16.8 Ω. These tests are presented in Video S3, and the final crumpled CNT printed wire is shown in Figure 5f. These demonstrations clearly show that the DWCNT printed wires are very resilient to any deformation.

■ CONCLUSIONS

Carbon nanotubes are amazing materials that are not only conducting but also very strong, flexible, and chemically stable.

Their large-scale industrial adoption has been hampered due to the unavailability of an industrially compatible process which can produce very high conductivity CNT dispersions, which do not require toxic/hazardous materials like acid and strong solvents. This work presents a very scalable process that produces one of the highest conductivity ($(3.6 \pm 0.2) \times 10^5$ S m^{-1}) and lowest sheet resistance ($\sim$0.11 $\Omega\ \square^{-1}$ mil^{-1}) CNT conducting films. The CNT films produced by using this dispersion have a decent thermal conductivity of 43 ± 4 W m^{-1} K^{-1}. Most importantly, we achieved this without using hazardous materials, and our method involves only a one-step dispersion process. The solvent and dispersion agent used in our process are water and cellulose (Na-CMC), respectively, which are not only nonhazardous but also abundant in nature. The microfluidization process presented in this work can be scaled up to produce CNT dispersions of hundreds of liters per day. Simplicity and scalability make this process very attractive for industrial adoption.

METHODS

Materials. DWCNTs were purchased from nanografi (www.nanografi.com). The average length was 48 μm, and the outer diameter was from 2 to 4 nm. CNTs were grown by using CVD. The ash weight was 1.5 wt %. Sodium carboxymethyl cellulose (Na CMC) had a MW $\sim$ 700000, and it was purchased from Sigma-Aldrich and had a carboxymethyl ($-OCH_2COO^-\ Na^+$) substitution of 0.9.

Microfluidization. Microfluidization is performed by using an LM20 microfluidizer. It is installed with a Z-type H210Z single microchannel, which has a hydraulic diameter of 200 μm. First, the solution is prepared by mixing 0.5 wt % DWCNTs and 0.3 wt % of Na-CMC in a deionized (DI) water and magnetic stirred overnight. For dispersion, the solution was poured into the MF reservoir, and the system was set to 10000 psi. After the solution is passed through the microchannel, it was recycled to the reservoir. The number of hydraulic pushes were counted to determine the number of processing cycles.

Characterization. Micrographs of the dispersed DWCNTs were obtained by a Zeiss Orion Nanofab ion microscope, using helium ions at 30 keV at about 4 pA. An ion microscope provides much better edge resolution than a conventional scanning electron microscope and is therefore used for imaging CNTs. Raman spectroscopy measurements were performed at 532 nm by using Renishaw inVia Raman microscope. The viscosity of the solutions was measured at 25 °C by using a TA Instruments Discovery Hybrid rheometer. To obtain the flow curve, shear stress was increased from 2 to 1000 s^{-1} at a gap of 500 μm. TEM images were obtained by using FEI's Tecnai Osiris TEM working at 200 keV.

For electrical measurements, DWCNTs dispersions were blade coated into a long rectangular film of length L, thickness d, and width W on a glass substrate, as shown in the inset of Figure 4b. After deposition, DWCNT films were dried in ambient conditions, and no postheating was performed. Silver conducting paint was applied for making contact pads. Four probe measurements were performed to measure the conductance. Conductivity was measured after measuring the thickness of the printed films at multiple points by using a Dektak profilometer. Four probe resistance measurements were performed by using a Keithley 5200 SCS parameter analyzer.

ASSOCIATED CONTENT

ⓢ Supporting Information

The Supporting Information is available free of charge at https://pubs.acs.org/doi/10.1021/acsanm.0c02013.

Reynolds number and shear rate calculation, comparison of the conductivities of MWCNT, SWCNT, FWCNT, and graphene, TEM of dispersed DWCNTs and their distribution of diameter, FTIR measurements of

dispersed DWCNTs, Na-CMC, and after processing the ink with HNO$_3$, Raman shift of DWCNTs, details of the thermal conductivity measurements (PDF)

Video S1: DWCNT coating of a cotton filament (MP4)

Video S2: measurement of the coated filament (MP4)

Video S3: measurements of DWCNT conducting films on a paper (MP4)

AUTHOR INFORMATION

Corresponding Author

Atif Aziz — *Department of Engineering, Nanoscience Centre, University of Cambridge, Cambridge CB3 0FF, U.K.;* ⓘ orcid.org/0000-0003-3701-2008; Email: aa267@cam.ac.uk

Authors

Mohamed Basel Bazbouz — *Department of Engineering, Nanoscience Centre, University of Cambridge, Cambridge CB3 0FF, U.K.;* ⓘ orcid.org/0000-0002-0953-6691

Mark Edward Welland — *Department of Engineering, Nanoscience Centre, University of Cambridge, Cambridge CB3 0FF, U.K.*

Complete contact information is available at:
https://pubs.acs.org/10.1021/acsanm.0c02013

Author Contributions

A.A. conceived the idea and designed the experiment. A.A. and B.A. performed the microfluidization and gravimetric analysis of the dispersion. A.A. fabricated the devices, conducted the measurement, and analyzed the results. A.A., B.B., and M.W. took part in the discussions and contributed to the manuscript.

Notes

The authors declare no competing financial interest.

REFERENCES

(1) Kong, J.; Franklin, N. R.; Zhou, C.; Chapline, M.; Peng, S.; Cho, K.; Dai, H. Nanotube Molecular Wires as Chemical Sensors. *Science* **2000**, *287*, 622.

(2) Sireesha, M.; Babu, V. J.; Kiran, A. S. K.; Ramakrishna, S. A Review on Carbon Nanotubes in Biosensor Devices and Their Applications in Medicine. *Nanocomposites* **2018**, *4* (2), 36.

(3) Dillon, A. C.; Jones, K. M.; Bekkedahl, T. A.; Kiang, C. H.; Bethune, D. S.; Heben, M. J. Storage of Hydrogen in Single-Walled Carbon Nanotubes. *Nature* **1997**, *386*, 377.

(4) Chen, K.; Gao, W.; Emaminejad, S.; Kiriya, D.; Ota, H.; Yin, H.; Nyein, Y.; Takei, K.; Javey, A. Printed Carbon Nanotube Electronics and Sensor Systems. *Adv. Mater.* **2016**, *28*, 4397.

(5) De Volder, M. F. L.; Tawfick, S. H.; Baughman, R. H.; Hart, A. J. Carbon Nanotubes: Present and Future Commercial Applications. *Science* **2013**, *339*, 535.

(6) Yamada, T.; Hayamizu, Y.; Yamamoto, Y.; Yomogida, Y.; Izadi-Najafabadi, A.; Futaba, D. N.; Hata, K. A Stretchable Carbon Nanotube Strain Sensor for Human-Motion Detection. *Nat. Nanotechnol.* **2011**, *6*, 296.

(7) Kim, J. H.; Hwang, J.; Hwang, H. R.; Kim, H. S.; Lee, J. H.; Seo, J.; Shin, U. S.; Lee, S. Simple and Cost-Effective Method of Highly Conductive and Elastic Carbon Nanotube/Polydimethylsiloxane Composite for Wearable Electronics. *Sci. Rep.* **2018**, *8*, 1375.

(8) Daneshvar, F.; Aziz, A.; Abdelkader, A. M.; Zhang, T.; Sue, H.-J.; Welland, M. E. Porous SnO$_2$ − Cux O Nanocomposite Thin Film on Carbon Nanotubes as Electrodes for High Performance Supercapacitors. *Nanotechnology* **2019**, *30*, 015401.

(9) Baughman, R. H.; Cui, C.; Zakhidov, A. A.; Iqbal, Z.; Barisci, J. N.; Spinks, G. M.; Wallace, G. G.; Mazzoldi, A.; Rossi, D. De; Rinzler, A. G.; Jaschinski, O.; Roth, S.; Kertesz, M. Carbon Nanotube Actuators. *Science* **1999**, *284*, 1340.

(10) Wu, Z.; Chen, Z.; Du, X.; Logan, J. M.; Sippel, J.; Nikolou, M.; Kamaras, K.; Reynolds, J. R.; Tanner, D. B.; Hebard, A. F.; Rinzler, A. G. Transparent, Conductive Carbon Nanotube Films. *Science* **2004**, *305*, 1273.

(11) Behabtu, N.; Young, C. C.; Tsentalovich, D. E.; Kleinerman, O.; Wang, X.; Ma, A. W. K.; Bengio, E. A.; ter Waarbeek, R. F.; de Jong, J. J.; Hoogerwerf, R. E.; Fairchild, S. B.; Ferguson, J. B.; Maruyama, B.; Kono, J.; Talmon, Y.; Cohen, Y.; Otto, M. J.; Pasquali, M. Strong, Light, Multifunctional Fibers of Carbon Nanotubes with Ultrahigh Conductivity. *Science* **2013**, *339*, 182.

(12) Geckeler, K. E.; Premkumar, T. Carbon Nanotubes: Are They Dispersed or Dissolved in Liquids? *Nanoscale Res. Lett.* **2011**, *6*, 136.

(13) Zhao, Y.; Wei, J.; Vajtai, R.; Ajayan, P. M.; Barrera, E. V. Iodine Doped Carbon Nanotube Cables Exceeding Specific Electrical Conductivity of Metals. *Sci. Rep.* **2011**, *1*, 83.

(14) Carbon, M.; Parra-Vasquez, A. N. G.; Behabtu, N.; Green, Ḱ. M. J.; Pint, C. L.; Young, Ḱ. C. C.; Schmidt, J.; Kesselman, E.; Goyal, A.; Ajayan, P. M.; Cohen, Y.; Talmon, Y.; Hauge, R. H.; Pasquali, M. Spontaneous Dissolution of Ultralong Single and Multiwalled Carbon Nanotubes. *ACS Nano* **2010**, *4* (7), 3969−3978.

(15) Menon, H.; Surendran, K. P. Screen Printable MWCNT Inks for Printed Electronics. *RSC Adv.* **2017**, *7*, 44076.

(16) Hu, L.; Choi, J. W.; Yang, Y.; Jeong, S.; La Mantia, F.; Cui, L.-F.; Cui, Y. Highly Conductive Paper for Energy-Storage Devices. *Proc. Natl. Acad. Sci. U. S. A.* **2009**, *106* (51), 21490.

(17) Preston, C.; Song, D.; Dai, J.; Tsinas, Z.; Bavier, J.; Cumings, J.; Ballarotto, V.; Hu, L. Scalable Nanomanufacturing of Surfactant-Free Carbon Nanotube Inks for Spray Coatings with High Conductivity. *Nano Res.* **2015**, *8* (7), 2242.

(18) Pan, K.; Fan, Y.; Leng, T.; Li, J.; Xin, Z.; Zhang, J.; Hao, L.; Gallop, J.; Novoselov, K. S.; Hu, Z. Sustainable Production of High Conductivity Multilayer Graphene Ink for Wireless Connectivity and IoT Applications. *Nat. Commun.* **2018**, *9*, 5197.

(19) Karagiannidis, P. G.; Hodge, S. A.; Lombardi, L.; Tomarchio, F.; Decorde, N.; Milana, S.; Goykhman, I.; Su, Y.; Mesite, S. V.; Johnstone, D. N.; Leary, R. K.; Midgley, P. A.; Pugno, N. M.; Torrisi, F.; Ferrari, A. C. Micro Fluidization of Graphite and Formulation of Graphene-Based Conductive Inks. *ACS Nano* **2017**, *11*, 2742.

(20) Leonard, N.; Guohua, H.; Richard, H.; Xiaoxi, Z.; Zongyin, T.; Jones, C.; Hasan, T. *Printing of Graphene and Related 2D Materials*; Springer International Publishing: Cham, 2019.

(21) Kharissova, O. V.; Kharisov, B. I.; de Casas Ortiz, E. G. Dispersion of Carbon Nanotubes in Water and Non-Aqueous Solvents. *RSC Adv.* **2013**, *3*, 24812.

(22) *Ultrasound in Chemistry*; Santos, H. M., Lodeiro, C., Capelo-Martinez, J. L., Eds.; Wiley-VCH Verlag GmbH & Co. KGaA: Weinheim, 2009; Chapter 1, pp 1−15.

(23) Cheng, Q.; Debnath, S.; Gregan, E.; Byrne, H. J. Ultrasound-Assisted SWNTs Dispersion: Effects of Sonication Parameters and Solvent Properties. *J. Phys. Chem. C* **2010**, *114* (19), 8821.

(24) Paton, K. R.; Varrla, E..; Coleman, J. N. Scalable Production of Large Quantities of Defect-Free Few-Layers Graphene by Shear Exfoliation in Liquids. *Nat. Mater.* **2014**, *13*, 624.

(25) Varrla, E.; Paton, K. R.; Backes, C.; Harvey, A.; Smith, R. J.; McCauley, J.; Coleman, J. N. Turbulence-Assisted Shear Exfoliation of Graphene Using Household Detergent and a Kitchen Blender. *Nanoscale* **2014**, *6*, 11810−11819.

(26) Roynolds, O. An Experimental Investigation of the Circumstances Which Determine Whether the Motion of Water Shall He Direct or Sinuous, and of the Law of Resistance in Parallel Channels. By. *Philos. Trans. R. Soc.* **1883**, *174*, 935.

(27) Yang, X. H.; Zhu, W. L. Viscosity Properties of Sodium Carboxymethylcellulose Solutions. *Cellulose* **2007**, *14*, 409−417.

(28) Minami, N.; Kim, Y.; Miyashita, K.; Kazaoui, S.; Nalini, B. Cellulose Derivatives as Excellent Dispersants for Single-Wall Carbon Nanotubes as Demonstrated by Absorption and Photoluminescence Spectroscopy. *Appl. Phys. Lett.* **2006**, *88*, 093123.

(29) Luo, S.; Liu, T.; Wang, Y.; Li, L.; Wang, G.; Luo, Y. Combined Microfluidization and Ultrasonication: A Synergistic Protocol for High-Efficient Processing of SWCNT Dispersions with High Quality. *J. Nanopart. Res.* **2016**, *18* (8), 1.

(30) Microfluidics Corp. US www.microfluidicscorp.com.

(31) Yanniotis, S.; Skaltsi, S.; Karaburnioti, S. Effect of Moisture Content on the Viscosity of Honey at Different Temperatures. *J. Food Eng.* **2006**, *72*, 372.

(32) He, G.; Messina, R.; Löwen, H.; Kiriy, A.; Bocharovab, V.; Stammb, M. Shear-Induced Stretching of Adsorbed Polymer Chains. *Soft Matter* **2009**, *5*, 3014−3017.

(33) Ma, A. W. K.; Chinesta, F.; Mackley, M. R. The Rheology and Modeling of Chemically Treated Carbon Nanotubes Suspensions Published by the The Society of Rheology The Rheology and Modeling of Chemically Treated Carbon Nanotubes Suspensions. *J. Rheol.* **2009**, *53* (3), 547.

(34) Muller, F. L.; Davidson, J. F. Rheology of Shear Thinning Polymer Solutions. *Ind. Eng. Chem. Res.* **1994**, *33*, 2364.